Available online at www.sciencedirect.com
SCIENCE DIRECT®
International Journal of Solids and Structures 42 (2005) 3439–3457
INTERNATIONAL JOURNAL OF SOLIDS and STRUCTURES
www.elsevier.com/locate/ijsolstr

# A constitutive model for shape memory alloys considering tensile–compressive asymmetry and plasticity

Alberto Paiva [a], Marcelo Amorim Savi [b,*], Arthur Martins Barbosa Braga [a], Pedro Manuel Calas Lopes Pacheco [c]

[a] *Department of Mechanical Engineering, Pontifícia Universidade Católica do Rio de Janeiro 22.453.900 Rio de Janeiro, RJ, Brazil*
[b] *COPPE—Department of Mechanical Engineering, Universidade Federal do Rio de Janeiro, Caixa Postal 68.503, 21.945.970 Rio de Janeiro, RJ, Brazil*
[c] *Department of Mechanical Engineering, CEFET/RJ, 20.271.110 Rio de Janeiro, RJ, Brazil*

Received 4 May 2004; received in revised form 5 November 2004
Available online 21 December 2004

**Abstract**

Shape memory alloys (SMAs) are materials that present, among other characteristics, the capacity to undergo large permanent strains, and then, after a proper increase on the temperature, recover its original shape. Constitutive models consider phenomenological aspects of thermomechanical behavior of these alloys. The present contribution proposes a constitutive model to consider both the tensile–compressive asymmetry and plastic strains that occur in the thermomechanical behavior of SMAs. A numerical procedure is proposed in order to deal with nonlinearities of the formulation. Comparisons between experimental and numerical results predicted by the proposed model show that they are in close agreement. Moreover, numerical simulations show that the model is capable to capture the general behavior of SMAs, allowing the description of important characteristics of these alloys as pseudo-elasticity, one-way and two-way shape memory effect, phase transformation due to temperature variations, internal sub-loops due to incomplete phase transformations and tensile–compressive asymmetry.


*Keywords:* Shape memory alloys; Constitutive model; Tensile-compressive asymmetry

* Corresponding author. Tel.: +55 21 25628372; fax: +55 21 25628383.
*E-mail addresses:* savi@ufrj.br (M.A. Savi), abraga@mec.puc-rio.br (A.M.B. Braga), calas@cefet-rj.br (P.M.C.L. Pacheco).

0020-7683/$ - see front matter © 2004 Elsevier Ltd. All rights reserved.
doi:10.1016/j.ijsolstr.2004.11.006

## 1. Introduction

Inspired by nature, researchers are trying to create systems and structures that can repair themselves, presenting an adaptive behavior according to its environment. Among many options of smart sensors and actuators employed in this kind of system, one can highlight shape memory alloys (SMAs). These alloys have the ability to return to a previous shape or dimension, when subjected to an appropriate thermomechanical procedure.

The remarkable properties of SMAs are attracting much technological interest, motivating different applications in several fields of sciences and engineering. They are ideally suited for use as fasteners, seals, connectors and clamps (van Humbeeck, 1999). Self-actuating fasteners, thermally actuator switches and several bioengineering devices are some examples of these applications (Machado and Savi, 2002, 2003; Duerig et al., 1999; Lagoudas et al., 1999). The use of SMAs can help solving many important problems in aerospace technology, in particular those concerning with space savings achieved by self-erectable structures and non-explosive release devices (Denoyer et al., 2000; Pacheco and Savi, 1997). Micromanipulators and robotics actuators have been built employing SMA properties to mimic the smooth motions of human muscles (Garner et al., 2001; Webb et al., 2000; Rogers, 1995). Moreover, SMAs are being used as actuators for vibration and buckling control of flexible structures. In this particular field, SMA wires embedded in composite materials have been used to modify mechanical characteristics of slender structures (Birman, 1997; Rogers, 1995). The main drawback of SMAs is their slow rate of change.

Metallurgical studies have revealed the microstructural aspects of the behavior of SMAs (Otsuka and Ren, 1999; Shaw and Kyriakides, 1995). Basically, there are two possible phases on SMAs: austenite and martensite. In martensitic phase, there are plates that may be internally twin related. Hence, different deformation orientations of crystallographic plates constitute what is known by martensitic variants. On SMAs there are 24 possible martensitic variants that are arranged in six plate groups with four plate variants per group (Zhang et al., 1991). Schroeder and Wayman (1977) have shown that for a temperature where martensite is the only stable phase in a stress-free state, when a specimen is deformed with increasing stress, only one of the four variants in a given plate group will begin to grow. This variant is the one that has the largest partial shear stress. On the other hand, because the crystal structure of martensite is less symmetric than the austenite, only a single variant is created on the reverse transformation (Zhang et al., 1991). For the analysis of one-dimensional media, it is possible to consider only three variants of martensite together with austenite ($A$) on SMAs: the twinned martensite ($M$), which is stable in the absence of a stress field, and two other martensitic phases ($M+$ and $M-$), which are induced by positive and negative stress fields, respectively.

Experimental results also show that SMAs present an asymmetric behavior when subjected to tensile or compressive loads. Polycrystalline NiTi, for example, deformed under compression, presents smaller recoverable strain levels, higher critical transformation stress levels, and steeper transformation stress–strain slopes (Gall et al., 1999). Gall and Sehitoglu (1999) argued that the tension–compression asymmetry in polycrystalline NiTi is caused by asymmetry at the single crystal level. Therefore, single crystal SMAs are expected to exhibit a considerable tension–compression asymmetry since their martensite habit planes present a very low symmetry with respect to the parent phase.

Other important phenomenon related to SMAs thermomechanical behavior is the plasticity. Plastic strains are concerned in different articles in order to evaluate either effects of these strains in phase transformations or the description of the two-way shape memory effect (Miller and Lagoudas, 2000). The loss of actuation through repeated cycling due to plastic strain development is one of the important aspects related to the effect of plastic strains in SMAs.

The thermomechanical behavior of shape memory alloys may be modeled either by microscopic or macroscopic point of view. There are many different works dedicated to the constitutive description of

the thermomechanical behavior of shape memory alloys and, despite the large number of applications, the modeling of SMA is still the objective of many researches developed in order to describe all details of its thermomechanical behavior (James, 2000; Savi et al., 2002).

This article presents a constitutive model for the description of the thermomechanical behavior of SMAs. The proposed model is based on the Fremond's theory (Fremond, 1987, 1996), later modified by Savi et al. (2002) and Baêta-Neves et al. (2004). Here, the tensile–compressive asymmetry is concerned allowing a correct description of the thermomechanical response of SMAs. The proposed model includes four macroscopic phases in the formulation: three variants of martensite and an austenitic phase. Plastic strain is included into the model and hardening effect is represented by a combination of kinematic and isotropic behaviors. An iterative numerical procedure based on the operator split technique (Ortiz et al., 1983), the orthogonal projection algorithm (Savi et al., 2002) and the return mapping algorithm (Simo and Hughes, 1998) is developed. Numerical results are carried out showing good agreements with experimental data.

## 2. Constitutive model

Fremond (1987, 1996) has proposed a three-dimensional model for the thermomechanical response of SMA where martensitic transformations are described with the aid of two internal variables. These variables represent volumetric fractions of two variants of martensite ($M+$ and $M-$), and must satisfy constraints regarding the coexistence of three distinct phases, the third being the parent austenitic phase ($A$). Savi et al. (2002) proposes a constitutive model built upon Fremond's original model including a fourth phase related to twinned martensite ($M$). Moreover, the proposed model introduces the description of plastic strain, considering a thermo-plastic-phase transformation coupling, and also different parameters for each phase. Recently, Baêta-Neves et al. (2004) proposes the enlargement of the stress–strain hysteresis loop in order to allow better adjustment to experimental data. This contribution revisits the cited model including tensile–compressive asymmetry.

Modeling of SMA behavior can be done within the scope of standard generalized materials (Lemaitre and Chaboche, 1990). With this assumption, the thermomechanical behavior can be described by the Helmholtz free energy, $\psi$, and the pseudo-potential of dissipation, $\Phi$. Therefore, the thermodynamic state is completely defined by a finite number of state variables: total strain, $\varepsilon$, temperature, $T$, the volumetric fractions of martensitic variants, $\beta_1$ and $\beta_2$, which are associated with detwinned martensites ($M+$ and $M-$, respectively) and austenite ($A$), $\beta_3$. The fourth phase is associated with twinned martensite ($M$) and its volumetric fraction is $\beta_4$. It should be pointed out that, macroscopically speaking, $A$, $M$, $M+$ and $M-$ are considered as different phases. The plastic phenomenon is described with the aid of plastic strain, $\varepsilon_p$, and the hardening effect is represented by a combination of kinematic and isotropic behaviors, described by variables $\mu$ and $\gamma$, respectively. With these assumptions, each phase have a free energy function as follows:

$$M+: \quad \rho\psi_1(\varepsilon_e, T, \gamma, \mu) = \frac{1}{2}E_M\varepsilon_e^2 - \alpha^T\varepsilon_e - \Lambda_M^T - \Omega_M(T - T_0)\varepsilon_e + \frac{1}{2}K_M\gamma^2 + \frac{1}{2H_M}\mu^2 \tag{1}$$

$$M-: \quad \rho\psi_2(\varepsilon_e, T, \gamma, \mu) = \frac{1}{2}E_M\varepsilon_e^2 + \alpha^C\varepsilon_e - \Lambda_M^C - \Omega_M(T - T_0)\varepsilon_e + \frac{1}{2}K_M\gamma^2 + \frac{1}{2H_M}\mu^2 \tag{2}$$

$$A: \quad \rho\psi_3(\varepsilon_e, T, \gamma, \mu) = \frac{1}{2}E_A\varepsilon_e^2 - \Lambda_A - \Omega_A(T - T_0)\varepsilon_e + \frac{1}{2}K_A\gamma^2 + \frac{1}{2H_A}\mu^2 \tag{3}$$

$$M: \quad \rho\psi_4(\varepsilon_e, T, \gamma, \mu) = \frac{1}{2}E_M\varepsilon_e^2 + \Lambda_M - \Omega_M(T - T_0)\varepsilon_e + \frac{1}{2}K_M\gamma^2 + \frac{1}{2H_M}\mu^2 \tag{4}$$

In the previous equations, subscript $M$ is related to martensitic phase while $A$ is associated with austenite. Moreover, superscript $T$ is related to tensile parameters while $C$ is associated with compressive parameters. Observing these indexes, notice that $\alpha$ is a material parameter related to the stress–strain hysteresis loop height observed during the martensitic transformation, while $\Lambda = \Lambda(T)$ are functions of temperature also related to the phase transformation; $E$ represents the elastic modulus, $\Omega$ is related to the thermal expansion coefficient, $K$ is the plastic modulus while $H$ is the kinematic hardening modulus; $T_0$ is a reference temperature and $\rho$ is the density. A free energy for the mixture can be written as follows:

$$\rho\widehat{\psi}(\varepsilon_e, T, \gamma, \mu, \beta_1, \beta_2, \beta_3, \beta_4) = \rho\sum_{i=1}^{4}\beta_i\psi_i(\varepsilon_e, T, \gamma, \mu) + \widehat{J}(\beta_1, \beta_2, \beta_3, \beta_4) \tag{5}$$

where $\widehat{J}(\beta_1, \beta_2, \beta_3, \beta_4)$ represents an indicator function related to the coexistence of four distinct phases, which is represented by constraints regarding:

$$0 \leqslant \beta_i \leqslant 1 \quad (i = 1, 2, 3, 4); \;\; \beta_1 + \beta_2 + \beta_3 + \beta_4 = 1 \tag{6}$$

Using this constraint, $\beta_4$ can be eliminated and the free energy can be rewritten as:

$$\rho\psi(\varepsilon_e, T, \gamma, \mu, \beta_1, \beta_2, \beta_3) = \rho\widetilde{\psi}(\varepsilon_e, T, \gamma, \mu, \beta_1, \beta_2, \beta_3) + J_\pi(\beta_1, \beta_2, \beta_3) \tag{7}$$

where,

$$\begin{aligned}
&\rho\widetilde{\psi}(\varepsilon_e, T, \gamma, \mu, \beta_1, \beta_2, \beta_3) \\
&\quad = \beta_1[-\alpha^T\varepsilon_e - (\Lambda_M + \Lambda_M^T)] + \beta_2[\alpha^C\varepsilon_e - (\Lambda_M + \Lambda_M^C)] \\
&\qquad + \beta_3\left[\frac{1}{2}(E_A - E_M)\varepsilon_e^2 - (\Lambda_M + \Lambda_A) - (\Omega_A - \Omega_M)(T - T_0)\varepsilon_e + \frac{1}{2}(K_A - K_M)\gamma^2 + \left(\frac{1}{2H_A} - \frac{1}{2H_M}\right)\mu^2\right] \\
&\qquad + \frac{1}{2}E_M\varepsilon_e^2 + \Lambda_M - \Omega_M(T - T_0)\varepsilon_e + \frac{1}{2}K_M\gamma^2 + \frac{1}{2H_M}\mu^2
\end{aligned} \tag{8}$$

and $J_\pi$ represents the indicator function given by the following convex set $\pi$, which can be geometrically represented by the tetrahedron presented in Fig. 1.

$$\pi = \{\beta_i \in \Re \mid 0 \leqslant \beta_i \leqslant 1 \quad (i = 1, 2, 3); \;\; \beta_1 + \beta_2 + \beta_3 \leqslant 1\} \tag{9}$$

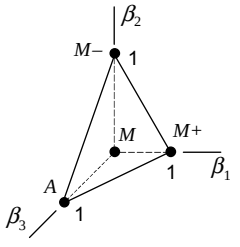


Fig. 1. Tetrahedron of the constraints $\pi$.

At this point, additive decomposition is assumed:

$$\varepsilon_{\mathrm{e}} = \varepsilon - \varepsilon_{\mathrm{p}} + \alpha_{\mathrm{h}}^{C}\beta_2 - \alpha_{\mathrm{h}}^{T}\beta_1 \tag{10}$$

where $\alpha_{\mathrm{h}}^{T}$ and $\alpha_{\mathrm{h}}^{C}$ are parameters associated with the stress–strain hysteresis loop width for tension and compression states, respectively. Under this assumption, the differential part of the free energy is rewritten as follows:

$$\begin{aligned}
&\rho\widetilde{\psi}(\varepsilon,\varepsilon_{\mathrm{p}},T,\gamma,\mu,\beta_1,\beta_2,\beta_3)\\
&\quad=\beta_1[-\alpha^{T}(\varepsilon-\varepsilon_{\mathrm{p}}+\alpha_{\mathrm{h}}^{C}\beta_2-\alpha_{\mathrm{h}}^{T}\beta_1)-(\Lambda_{\mathrm{M}}+\Lambda_{\mathrm{M}}^{T})]+\beta_2[\alpha^{C}(\varepsilon-\varepsilon_{\mathrm{p}}+\alpha_{\mathrm{h}}^{C}\beta_2-\alpha_{\mathrm{h}}^{T}\beta_1)-(\Lambda_{\mathrm{M}}+\Lambda_{\mathrm{M}}^{C})]\\
&\qquad+\beta_3\left[\frac{1}{2}(E_{\mathrm{A}}-E_{\mathrm{M}})(\varepsilon-\varepsilon_{\mathrm{p}}+\alpha_{\mathrm{h}}^{C}\beta_2-\alpha_{\mathrm{h}}^{T}\beta_1)^2-(\Lambda_{\mathrm{A}}+\Lambda_{\mathrm{M}})-(\Omega_{\mathrm{A}}-\Omega_{\mathrm{M}})(T-T_0)(\varepsilon-\varepsilon_{\mathrm{p}}+\alpha_{\mathrm{h}}^{C}\beta_2-\alpha_{\mathrm{h}}^{T}\beta_1)\right.\\
&\qquad\left.+\frac{1}{2}(K_{\mathrm{A}}-K_{\mathrm{M}})\gamma^2+\left(\frac{1}{2H_{\mathrm{A}}}-\frac{1}{2H_{\mathrm{M}}}\right)\mu^2\right]+\frac{1}{2}E_{\mathrm{M}}(\varepsilon-\varepsilon_{\mathrm{p}}+\alpha_{\mathrm{h}}^{C}\beta_2-\alpha_{\mathrm{h}}^{T}\beta_1)^2+\Lambda_{\mathrm{M}}-\Omega_{\mathrm{M}}(T-T_0)(\varepsilon-\varepsilon_{\mathrm{p}}\\
&\qquad+\alpha_{\mathrm{h}}^{C}\beta_2-\alpha_{\mathrm{h}}^{T}\beta_1)+\frac{1}{2}K_{\mathrm{M}}\gamma^2+\frac{1}{2H_{\mathrm{M}}}\mu^2
\end{aligned} \tag{11}$$

State equations can be obtained from the Helmholtz free energy as follows:

$$\sigma=\rho\frac{\partial\psi}{\partial\varepsilon}=E(\varepsilon-\varepsilon_{\mathrm{p}}+\alpha_{\mathrm{h}}^{C}\beta_2-\alpha_{\mathrm{h}}^{T}\beta_1)+\alpha^{C}\beta_2-\alpha^{T}\beta_1-\Omega(T-T_0) \tag{12}$$

$$\begin{aligned}
B_1\in-\rho\partial_1\psi=\alpha^{T}(\varepsilon-\varepsilon_{\mathrm{p}})+\Lambda_1+\beta_2(\alpha_{\mathrm{h}}^{C}\alpha^{T}+\alpha_{\mathrm{h}}^{T}\alpha^{C}+E\alpha_{\mathrm{h}}^{T}\alpha_{\mathrm{h}}^{C})-\beta_1(2\alpha_{\mathrm{h}}^{T}\alpha^{T}+E\alpha_{\mathrm{h}}^{T^2})\\
+\alpha_{\mathrm{h}}^{T}[E(\varepsilon-\varepsilon_{\mathrm{p}})-\Omega(T-T_0)]-\partial_1 J_\pi
\end{aligned} \tag{13}$$

$$\begin{aligned}
B_2\in-\rho\partial_2\psi=-\alpha^{C}(\varepsilon-\varepsilon_{\mathrm{p}})+\Lambda_2+\beta_1(\alpha_{\mathrm{h}}^{T}\alpha^{C}+\alpha_{\mathrm{h}}^{C}\alpha^{T}+E\alpha_{\mathrm{h}}^{C}\alpha_{\mathrm{h}}^{T})-\beta_2(2\alpha_{\mathrm{h}}^{C}\alpha^{C}+E\alpha_{\mathrm{h}}^{C^2})\\
-\alpha_{\mathrm{h}}^{C}[E(\varepsilon-\varepsilon_{\mathrm{p}})-\Omega(T-T_0)]-\partial_2 J_\pi
\end{aligned} \tag{14}$$

$$\begin{aligned}
B_3\in-\rho\partial_3\psi=-\frac{1}{2}(E_{\mathrm{A}}-E_{\mathrm{M}})(\varepsilon-\varepsilon_{\mathrm{p}}+\alpha_{\mathrm{h}}^{C}\beta_2-\alpha_{\mathrm{h}}^{T}\beta_1)^2+\Lambda_3+(\Omega_{\mathrm{A}}-\Omega_{\mathrm{M}})(T-T_0)(\varepsilon-\varepsilon_{\mathrm{p}}+\alpha_{\mathrm{h}}^{C}\beta_2-\alpha_{\mathrm{h}}^{T}\beta_1)\\
-\frac{1}{2}(K_{\mathrm{A}}-K_{\mathrm{M}})\gamma^2-\left(\frac{1}{2H_{\mathrm{A}}}-\frac{1}{2H_{\mathrm{M}}}\right)\mu^2-\partial_3 J_\pi
\end{aligned} \tag{15}$$

$$X=-\rho\frac{\partial\psi}{\partial\varepsilon_{\mathrm{p}}}=E(\varepsilon-\varepsilon_{\mathrm{p}}+\alpha_{\mathrm{h}}^{C}\beta_2-\alpha_{\mathrm{h}}^{T}\beta_1)+\alpha^{C}\beta_2-\alpha^{T}\beta_1-\Omega(T-T_0)=\sigma \tag{16}$$

$$Y=-\rho\frac{\partial\psi}{\partial\gamma}=-K\gamma \tag{17}$$

$$Z=-\rho\frac{\partial\psi}{\partial\mu}=-\frac{1}{H}\mu \tag{18}$$

where $B_i$, $X$, $Y$ and $Z$ are thermodynamic forces, $\sigma$ represents the uniaxial stress and $\partial_i J_\pi$ are the sub-differentials with respect to $\beta_i$ (Rockafellar, 1970). Lagrange multipliers offer a good alternative to represent

sub-differentials of the indicator function (Savi and Braga, 1993). Furthermore, the parameters $E$, $\Omega$, $K$ and $H$ are defined from their correspondent values for austenitic and martensitic phases, as follows:

$$E = E_{\mathrm{M}} - \beta_3(E_{\mathrm{M}} - E_{\mathrm{A}}) \tag{19}$$

$$\Omega = \Omega_{\mathrm{M}} - \beta_3(\Omega_{\mathrm{M}} - \Omega_{\mathrm{A}}) \tag{20}$$

$$K = K_{\mathrm{M}} - \beta_3(K_{\mathrm{M}} - K_{\mathrm{A}}) \tag{21}$$

$$\frac{1}{H} = \frac{1}{H_{\mathrm{M}}} - \beta_3\left(\frac{1}{H_{\mathrm{M}}} - \frac{1}{H_{\mathrm{A}}}\right) \tag{22}$$

and functions $\Lambda_1$, $\Lambda_2$ and $\Lambda_3$ are defined as:

$$\Lambda_1 = \Lambda_1(T) = \Lambda_{\mathrm{M}} + \Lambda_{\mathrm{M}}^{T} \tag{23}$$

$$\Lambda_2 = \Lambda_2(T) = \Lambda_{\mathrm{M}} + \Lambda_{\mathrm{M}}^{C} \tag{24}$$

$$\Lambda_3 = \Lambda_3(T) = \Lambda_{\mathrm{M}} + \Lambda_{\mathrm{A}} \tag{25}$$

In order to describe the dissipation processes, it is necessary to introduce a pseudo-potential of dissipation $\Phi$. In general, it is possible to make a decomposition of the form:

$$\Phi = \Phi(\dot{\varepsilon}, \dot{\varepsilon}_{\mathrm{p}}, \dot{\mu}, \dot{\gamma}, \dot{\beta}_i, q) = \phi(\dot{\varepsilon}, \dot{\varepsilon}_{\mathrm{p}}, \dot{\mu}, \dot{\gamma}, \dot{\beta}_i) + \phi_q(q) \tag{26}$$

Here, the interest is focused on the mechanical part of the potential and, for convenience, is expressed in terms of its dual $\phi^* = \phi^*(B_i, X, Y, Z)$:

$$\phi^* = \frac{1}{2\eta_1}(B_1 + \eta_{\mathrm{ci}}Y + \eta_{\mathrm{ck}}Z)^2 + \frac{1}{2\eta_2}(B_2 + \eta_{\mathrm{ci}}Y + \eta_{\mathrm{ck}}Z)^2 + \frac{1}{2\eta_3}(B_3 - \eta_{\mathrm{ci}}Y - \eta_{\mathrm{ck}}Z)^2 + J_\chi(B_1, B_2, B_3) + J_{\mathrm{f}}(X, Y, Z) \tag{27}$$

where $J_{\mathrm{f}}$ is the indicator function related to the yield surface defined as follows:

$$f = |\, X + HZ \,| - (\sigma_Y - Y) \text{ or } f(\sigma, \mu, \gamma) = |\, \sigma - \mu \,| - (\sigma_Y + K\gamma) \tag{28}$$

while $J_\chi$ is the indicator function related to the convex set $\chi$, which provide constraints associated with phase transformations evolution. Physically, this indicator function establishes constraints related to internal sub-loops due to incomplete phase transformations and also to the formation of detwinned martensite ($M$). Hence, defining

$$\varepsilon_0 = \varepsilon - \frac{\Omega}{E}(T - T_0) \tag{29}$$

the convex set $\chi$ may be written as follows for a mechanical loading history with $\dot{\sigma} \neq 0$:

$$\chi = \left\{ \dot{\beta}_n \in \Re \,\middle|\, \begin{array}{ll} \dot{\varepsilon}\dot{\beta}_1 \geqslant 0; & \dot{\varepsilon}\dot{\beta}_3 \leqslant 0 \quad \text{if } \varepsilon_0 > 0 \\ \dot{\varepsilon}\dot{\beta}_2 \leqslant 0; & \dot{\varepsilon}\dot{\beta}_3 \geqslant 0 \quad \text{if } \varepsilon_0 < 0 \end{array} \right\} \tag{30}$$

On the other hand, when $\dot{\sigma} = 0$, the convex set $\chi$ is expressed by

$$\chi = \left\{ \dot{\beta}_n \in \Re \left| \begin{array}{l} \dot{T}\dot{\beta}_1 \begin{cases} < 0 \text{ if } \dot{T} > 0, \sigma < \sigma_{\mathrm{M}}^{\mathrm{crit}} \text{ and } \beta_1^s \neq 0 \\ = 0 \text{ otherwise} \end{cases} \\ \dot{T}\dot{\beta}_2 \begin{cases} < 0 \text{ if } \dot{T} > 0, \sigma < \sigma_{\mathrm{M}}^{\mathrm{crit}} \text{ and } \beta_2^s \neq 0 \\ = 0 \text{ otherwise} \end{cases} \\ \dot{T}\dot{\beta}_3 \geqslant 0 \\ -\dot{\beta}_1^2 - \dot{\beta}_1\dot{\beta}_3 = 0 \text{ or } -\dot{\beta}_2^2 - \dot{\beta}_2\dot{\beta}_3 = 0 \end{array} \right. \right\} \tag{31}$$

where $\beta_1^s$ and $\beta_2^s$ are the values of $\beta_1$ and $\beta_2$ respectively, when the phase transformation begins to take place. Moreover, $\sigma_{\mathrm{M}}^{\mathrm{crit}}$, which actually has different values for tensile or compressive behaviors ($\sigma_{\mathrm{M}}^{T\mathrm{crit}}$ and $\sigma_{\mathrm{M}}^{C\mathrm{crit}}$), are the critical stress values for $M \to M+$ and $M \to M-$ phase transformations.

Together with constraints related to internal sub-loops, the set (31) also expresses a constraint to eliminate both $M+ \to M$ and $M- \to M$ phase transformations. In mathematical terms, this is expressed by $\dot{\beta}_1\dot{\beta}_4 = \dot{\beta}_1(-\dot{\beta}_1 - \dot{\beta}_2 - \dot{\beta}_3) = -\dot{\beta}_1^2 - \dot{\beta}_1\dot{\beta}_3 = 0$ or $\dot{\beta}_2\dot{\beta}_4 = \dot{\beta}_2(-\dot{\beta}_1 - \dot{\beta}_2 - \dot{\beta}_3) = -\dot{\beta}_2^2 - \dot{\beta}_2\dot{\beta}_3 = 0$, respectively, which means that when one kind of transformation occurs the other needs to vanish. Moreover, the discarded terms in both equations ($-\dot{\beta}_1\dot{\beta}_2$) represent impossible transformations to occur and, thus, are not considered.

The parameter $\eta_i$ ($i = 1, 2, 3$) is associated with the internal dissipation of the material while $\eta_{\mathrm{ci}}$ and $\eta_{\mathrm{ck}}$ are related to plastic-phase transformation coupling. The parameter $\eta_{\mathrm{ci}}$ is associated with isotropic hardening coupling while $\eta_{\mathrm{ck}}$ is associated with kinematic hardening coupling. At this point, it is possible to write the following complementary equations:

$$\dot{\beta}_1 \in \partial_{B_1}\phi = \frac{B_1}{\eta_1} + \frac{\eta_{\mathrm{ci}}}{\eta_1}Y + \frac{\eta_{\mathrm{ck}}}{\eta_1}Z + \partial_1 J_\chi = \frac{B_1}{\eta_1} - \frac{\eta_{\mathrm{ci}}}{\eta_1}K\gamma - \frac{\eta_{\mathrm{ck}}}{\eta_1}\frac{\mu}{H} + \partial_1 J_\chi \tag{32}$$

$$\dot{\beta}_2 \in \partial_{B_2}\phi = \frac{B_2}{\eta_2} + \frac{\eta_{\mathrm{ci}}}{\eta_2}Y + \frac{\eta_{\mathrm{ck}}}{\eta_2}Z + \partial_2 J_\chi = \frac{B_2}{\eta_2} - \frac{\eta_{\mathrm{ci}}}{\eta_2}K\gamma - \frac{\eta_{\mathrm{ck}}}{\eta_2}\frac{\mu}{H} + \partial_2 J_\chi \tag{33}$$

$$\dot{\beta}_3 \in \partial_{B_3}\phi = \frac{B_3}{\eta_3} - \frac{\eta_{\mathrm{ci}}}{\eta_3}Y - \frac{\eta_{\mathrm{ck}}}{\eta_3}Z + \partial_3 J_\chi = \frac{B_3}{\eta_3} + \frac{\eta_{\mathrm{ci}}}{\eta_3}K\gamma + \frac{\eta_{\mathrm{ck}}}{\eta_3}\frac{\mu}{H} + \partial_3 J_\chi \tag{34}$$

$$\dot{\varepsilon}_p \in \partial_X\phi = \lambda \text{ sign } (X + HZ) = \lambda \text{ sign } (\sigma - \mu) \tag{35}$$

$$\dot{\gamma} \in \partial_Y\phi = \lambda + \eta_{\mathrm{ci}}(\dot{\beta}_1 + \dot{\beta}_2 - \dot{\beta}_3) = |\ \dot{\varepsilon}_p\ | + \eta_{\mathrm{ci}}(\dot{\beta}_1 + \dot{\beta}_2 - \dot{\beta}_3) \tag{36}$$

$$\dot{\mu} \in \partial_Z\phi = \lambda H \text{ sign } (X + HZ) + \eta_{\mathrm{ck}}(\dot{\beta}_1 + \dot{\beta}_2 - \dot{\beta}_3) = H\dot{\varepsilon}_p + \eta_{\mathrm{ck}}(\dot{\beta}_1 + \dot{\beta}_2 - \dot{\beta}_3) \tag{37}$$

where $\lambda$ is the plastic multiplier and $\partial_i J_\chi$ are the sub-differentials with respect to variables $\dot{\beta}_i$. The irreversible nature of plastic flow is represented by means of the *Kuhn–Tucker conditions*. Another constraint must be satisfied when $f(\sigma, \gamma, \mu) = 0$, referred as the *consistency condition*. These conditions are presented as follows (Simo and Hughes, 1998):

$$\lambda \geqslant 0; \quad f(\sigma, \gamma, \mu) \leqslant 0; \quad \lambda f(\sigma, \gamma, \mu) = 0; \quad \lambda \dot{f}(\sigma, \gamma, \mu) = 0 \text{ if } f(\sigma, \gamma, \mu) = 0 \tag{38}$$

These equations form a complete set of constitutive equations. Since the pseudo-potential of dissipation is convex, positive and vanishes at the origin, the Clausius–Duhen inequality is automatically satisfied if the entropy is defined as $s = -\partial\psi/\partial T$. The following box summarizes the set of constitutive equations:

Box 1: Constitutive equations

$$\sigma = E(\varepsilon - \varepsilon_{\mathrm{p}} + \alpha_{\mathrm{h}}^{C}\beta_2 - \alpha_{\mathrm{h}}^{T}\beta_1) + \alpha^{C}\beta_2 - \alpha^{T}\beta_1 - \Omega(T - T_0)$$

$$\dot{\beta}_1 = \frac{1}{\eta_1}\left\{\alpha^{T}(\dot{\varepsilon} - \dot{\varepsilon}_{\mathrm{p}}) + \Lambda_1 + \beta_2(\alpha_{\mathrm{h}}^{C}\alpha^{T} + \alpha_{\mathrm{h}}^{T}\alpha^{C} + E\alpha_{\mathrm{h}}^{T}\alpha_{\mathrm{h}}^{C}) - \beta_1(2\alpha_{\mathrm{h}}^{T}\alpha^{T} + E\alpha_{\mathrm{h}}^{T^2}) - \alpha_{\mathrm{h}}^{T}[E(\varepsilon - \varepsilon_{\mathrm{p}}) - \Omega(T - T_0)] - \eta_{\mathrm{ci}}K\gamma - \eta_{\mathrm{ck}}\frac{\mu}{H} - \partial_1 J_{\pi}\right\} + \partial_1 J_{\chi}$$

$$\dot{\beta}_2 = \frac{1}{\eta_2}\left\{-\alpha^{C}(\dot{\varepsilon} - \dot{\varepsilon}_{\mathrm{p}}) + \Lambda_2 + \beta_1(\alpha_{\mathrm{h}}^{T}\alpha^{C} + \alpha_{\mathrm{h}}^{C}\alpha^{T} + E\alpha_{\mathrm{h}}^{C}\alpha_{\mathrm{h}}^{T}) - \beta_2(2\alpha_{\mathrm{h}}^{C}\alpha^{C} + E\alpha_{\mathrm{h}}^{C^2}) - \alpha_{\mathrm{h}}^{C}[E(\varepsilon - \varepsilon_{\mathrm{p}}) - \Omega(T - T_0)] - \eta_{\mathrm{ci}}K\gamma - \eta_{\mathrm{ck}}\frac{\mu}{H} - \partial_2 J_{\pi}\right\} + \partial_2 J_{\chi}$$

$$\dot{\beta}_3 = \frac{1}{\eta_3}\left\{-\frac{1}{2}(E_{\mathrm{A}} - E_{\mathrm{M}})(\varepsilon - \varepsilon_{\mathrm{p}} + \alpha_{\mathrm{h}}^{C}\beta_2 - \alpha_{\mathrm{h}}^{T}\beta_1)^2 + \Lambda_3 + (\Omega_{\mathrm{A}} - \Omega_{\mathrm{M}})(T - T_0)(\varepsilon - \varepsilon_{\mathrm{p}} + \alpha_{\mathrm{h}}^{C}\beta_2 - \alpha_{\mathrm{h}}^{T}\beta_1) - \frac{1}{2}(K_{\mathrm{A}} - K_{\mathrm{M}})\gamma^2 - \left(\frac{1}{2H_{\mathrm{A}}} - \frac{1}{2H_{\mathrm{M}}}\right)\mu^2 + \eta_{\mathrm{ci}}K\gamma + \eta_{\mathrm{ck}}\frac{\mu}{H} - \partial_3 J_{\pi}\right\} + \partial_3 J_{\chi}$$

$$\dot{\varepsilon}_{\mathrm{p}} = \lambda \ \mathrm{sign}\ (\sigma - \mu)$$

$$\dot{\gamma} = |\ \dot{\varepsilon}_{\mathrm{p}}\ | + \eta_{\mathrm{ci}}(\dot{\beta}_1 + \dot{\beta}_2 - \dot{\beta}_3)$$

$$\dot{\mu} = H\dot{\varepsilon}_p + \eta_{\mathrm{ck}}(\dot{\beta}_1 + \dot{\beta}_2 - \dot{\beta}_3)$$

### 2.1. Material parameters

This section presents a brief description about some material parameters related to the proposed model. A detailed description of these model parameters and also their sensitivity analysis may be found in Paiva (2004).

At first, it is important to consider the definition of the functions $\Lambda_1$, $\Lambda_2$ and $\Lambda_3$ which are temperature dependent as follows:

$$\Lambda_1 = -L_0^{T} + \frac{L^{T}}{T_{\mathrm{M}}}(T - T_{\mathrm{M}}) \tag{39}$$

$$\Lambda_2 = -L_0^{C} + \frac{L^{C}}{T_{\mathrm{M}}}(T - T_{\mathrm{M}}) \tag{40}$$

$$\Lambda_3 = -L_0^{A} + \frac{L^{A}}{T_{\mathrm{M}}}(T - T_{\mathrm{M}}) \tag{41}$$

Here, $T_{\mathrm{M}}$ is the temperature below which the martensitic phase becomes stable. Besides, $L_0^{T}$, $L^{T}$, $L_0^{C}$, $L^{C}$, $L_0^{A}$ and $L^{A}$ are parameters related to critical stress for phase transformation, remembering that the indexes $T$ refers to tensile, $C$ to compression and $A$ to austenite.

The definition of these functions establishes the phase transformation critical stress for each phase. Actually, the definition of critical stress is essential to evaluate the convex set $\chi$ when $\dot{\sigma} = 0$. It may be obtained from the two first equations presented in Box 1 considering $\dot{\beta}_1 = \beta_1 = \beta_2 = \beta_3 = 0$. Therefore, the following expression is obtained for tensile behavior

$$\sigma_{\mathrm{M}}^{T\mathrm{crit}} = \frac{E_{\mathrm{M}}}{\alpha^T + E_{\mathrm{M}}\alpha_{\mathrm{h}}^T}\left[L_0^T - \frac{L^T(T - T_{\mathrm{M}})}{T_{\mathrm{M}}} + \alpha_{\mathrm{h}}^T \Omega_{\mathrm{M}}(T - T_0) + \eta_{\mathrm{ci}} K_{\mathrm{M}}\gamma + \eta_{\mathrm{ck}}\frac{\mu}{H_{\mathrm{M}}}\right] - \Omega_{\mathrm{M}}(T - T_0) \tag{42}$$

Another important characteristic of the model is that there is a critical temperature, $T_C$, below which there is no change in stress–strain hysteresis loop position. This temperature limits the variation of the transformation critical stress and can be determined by evaluating again the two first constitutive equations in Box 1, assuming $\dot{\beta}_1 = \beta_2 = \beta_3 = 0; \beta_1 = 1;\ \varepsilon = \varepsilon_{\mathrm{R}}^T;\ \varepsilon_{\mathrm{p}} = 0;\ T = T_C^T$. Therefore, the following parameters are defined for tensile behavior,

$$\alpha_{\mathrm{h}}^T = \varepsilon_{\mathrm{R}}^T - \frac{\alpha^T}{E_{\mathrm{M}}} - \frac{\Omega_{\mathrm{M}}}{E_{\mathrm{M}}}(T_C^T - T_0), \qquad T_C^T = T_{\mathrm{M}}\left[\frac{(L_0^T + L^T)E_{\mathrm{M}} + \alpha^T(\Omega_{\mathrm{M}}T_0 - \alpha^T)}{L^T E_{\mathrm{M}} + \alpha^T \Omega_{\mathrm{M}} T_{\mathrm{M}}}\right] \tag{43}$$

As pointed before, the first parameter is related to the horizontal size of the stress–strain hysteresis loop for tensile behavior, which is function of the maximum residual strain $\varepsilon_{\mathrm{R}}^T$ that is a usual parameter obtained during SMAs' experimental characterization.

An analogous procedure considering the evolution of $\beta_2$ defines similar parameters for compressive behavior:

$$\sigma_{\mathrm{M}}^{C\mathrm{crit}} = \frac{E_{\mathrm{M}}}{\alpha^C + E_{\mathrm{M}}\alpha_{\mathrm{h}}^C}\left[-L_0^C + \frac{L^C(T - T_{\mathrm{M}})}{T_{\mathrm{M}}} + \alpha_{\mathrm{h}}^C \Omega_{\mathrm{M}}(T - T_0) - \eta_{\mathrm{ci}} K_{\mathrm{M}}\gamma - \eta_{\mathrm{ck}}\frac{\mu}{H_{\mathrm{M}}}\right] - \Omega_{\mathrm{M}}(T - T_0) \tag{44}$$

And also,

$$\alpha_{\mathrm{h}}^C = -\varepsilon_{\mathrm{R}}^C - \frac{\alpha^C}{E_{\mathrm{M}}} + \frac{\Omega_{\mathrm{M}}}{E_{\mathrm{M}}}\left(T_C^C - T_0\right), \qquad T_C^C = T_{\mathrm{M}}\left[\frac{(L_0^C + L^C)E_{\mathrm{M}} - \alpha^C(\Omega_{\mathrm{M}}T_0 + \alpha^T)}{L^C E_{\mathrm{M}} - \alpha^C \Omega_{\mathrm{M}} T_{\mathrm{M}}}\right] \tag{45}$$

Now, it should be pointed out that functions $\Lambda_1$, $\Lambda_2$ and $\Lambda_3$ do not vary for temperatures below these critical values.

In order to contemplate different characteristics to the kinetics of phase transformation for loading and unloading processes, it is possible to consider different values to the parameter $\eta_i$, which is related to internal dissipation. Therefore,

$$\begin{cases} \eta_i = \eta_i^L \text{ if } \dot{\varepsilon} > 0 \\ \eta_i = \eta_i^U \text{ if } \dot{\varepsilon} < 0 \end{cases} \tag{46}$$

where $\eta_i^L$ and $\eta_i^U$ are internal dissipation parameters related to variable $\beta_i$ during loading or unloading process, respectively.

The yield limit $\sigma_Y$ has different values for austenitic and martensitic phases. Moreover, for very high temperatures, this value tends to decrease. Therefore, it is assumed that the yield limit has a linear variation with $T$, evaluated with the following expression:

$$\begin{cases} \sigma_Y = \sigma_Y^M \text{ if } T \leqslant T_{\mathrm{M}} \\ \sigma_Y = \dfrac{\sigma_Y^M(T_{\mathrm{A}} - T) + \sigma_Y^{A,i}(T - T_{\mathrm{M}})}{T_{\mathrm{A}} - T_{\mathrm{M}}} \text{ if } T_{\mathrm{M}} < T \leqslant T_{\mathrm{A}} \\ \sigma_Y = \dfrac{\sigma_Y^{A,i}(T_F - T) + \sigma_Y^{A,f}(T - T_{\mathrm{A}})}{T_F - T_{\mathrm{A}}} \text{ if } T_{\mathrm{A}} < T \leqslant T_F \end{cases} \tag{47}$$

where $T_F$ is a reference temperature related to high values of temperature and $T_A$ is the temperature above which austenite is the only stable phase.

### 2.2. Numerical procedure

The operator split technique (Ortiz et al., 1983) associated with an iterative numerical procedure is developed in order to deal with the nonlinearities of the formulation. The procedure isolates the sub-differentials and uses the implicit Euler method combined with an orthogonal projection algorithm (Savi et al., 2002) to evaluate evolution equations. Orthogonal projections assure that volumetric fractions of the martensitic variants will obey the imposed constraints. In order to satisfy constraints expressed in (9), values of volumetric fractions must stay inside or on the boundary of $\pi$, the tetrahedron shown in Fig. 1. The elasto-plastic behavior is simulated with the aid of the classical return mapping algorithm proposed by Simo and Hughes (1998).

## 3. General thermomechanical behavior

This section presents a discussion about thermomechanical behavior of SMAs predicted by the proposed model. A SMA specimen subjected to tensile behavior is considered in this analysis. At first, the model parameters are adjusted, by comparing numerical results obtained with the proposed model with experimental results presented by Tobushi et al. (1991). After that, numerical simulations considering other thermomechanical loading processes are addressed in order to show the potentiality of the model to describe several complex thermomechanical behaviors.

### 3.1. Model calibration

The calibration of the proposed model is done comparing numerical simulation with experimental data presented by Tobushi et al. (1991), which describes tensile tests on Ni–Ti wires at different temperatures. Basically, three different temperatures are considered here: 333 K, 353 K and 373 K (Fig. 2). Notice that, even though this is a pseudo-elastic test, experimental data for $T = 373$ K and 353 K presents a residual

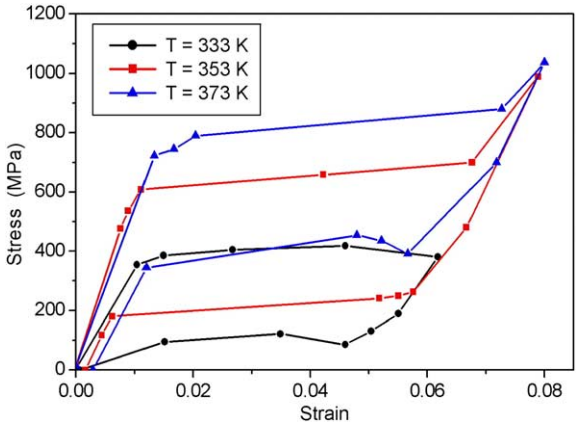


Fig. 2. Experimental stress–strain curves for a Ni–Ti SMA (Tobushi et al., 1991).

Table 1
Model parameters for a Ni–Ti SMA (Tobushi et al., 1991)

| $E_A$ (GPa) | $E_M$ (GPa) | $\Omega_A$ (MPa/K) | $\Omega_M$ (MPa/K) | $\alpha^T$ (MPa) | $L_0^T$ (MPa) | $L^T$ (MPa) | $L_0^A$ (MPa) | $L^A$ (MPa) | $\varepsilon_R^T$ | $\eta_1^L$ (MPa s) | $\eta_1^U$ (MPa s) | $\eta_3^L$ (MPa s) | $\eta_3^U$ (MPa s) | $T_M$ (K) | $T_A$ (K) | $T_0$ (K) |
|---|---|---|---|---|---|---|---|---|---|---|---|---|---|---|---|---|
| 54 | 42 | 0.74 | 0.17 | 330 | 0.15 | 41.5 | 0.63 | 185 | 0.0555 | 1 | 2.7 | 1 | 2.7 | 291.4 | 307.5 | 307 |

strain at the end of the loading–unloading process, which is probably related to transformation induced plasticity (Lagoudas et al., 2003).

Temperature $T = 373$ K is used to calibrate model parameters, in order to reproduce the experimental data. Table 1 presents the adjusted parameters. Since there is neither compression nor plasticity related to the cited test, the associated parameters are not presented. Fig. 3 shows both numerical and experimental data for the three temperatures, showing good agreements. The model does not predict residual strain after the loading–unloading process since yield surface is not reached (in spite of the residual strain observed in experimental data for $T = 373$ K and 353 K). Although the proposed model has a plastic-phase transformation coupling, this coupling only considers that plastic strains affect phase transformation and not vice versa. For $T = 333$ K, the experimental curve does not present an elastic response related to martensitic

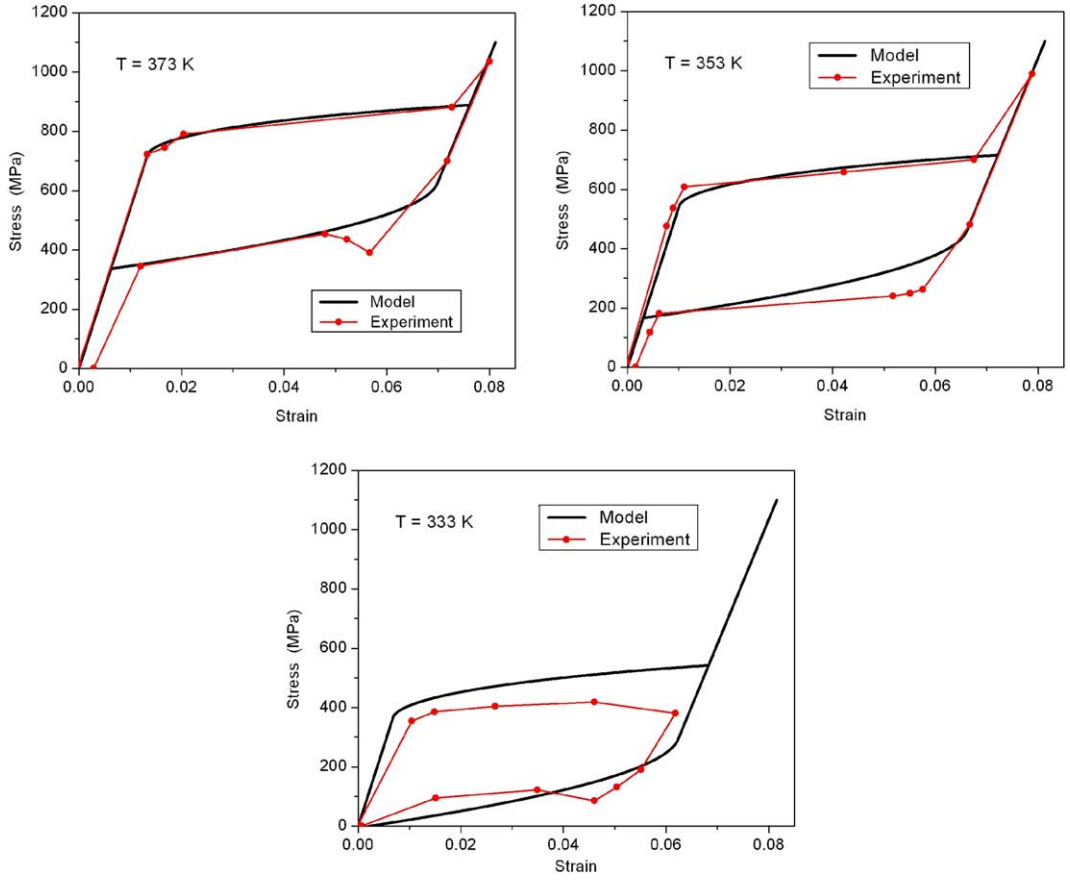


Fig. 3. Comparison between numerical and experimental results.

phase. Probably, this is associated with an incomplete phase transformation, which explains the little discrepancy between results. In general, it is possible to say that the proposed model captures the general behavior of SMAs, presenting good agreement with experimental data.

### 3.2. Numerical simulations of the general thermomechanical behavior of SMAs

This section presents some numerical simulations developed in order to illustrate the capacity of the model to capture the general thermomechanical behavior of SMAs. Basically, numerical results related to pseudo-elasticity, shape memory effect (one-way and two-way), phase transformation induced by temperature variation and internal sub-loops due to incomplete phase transformation are addressed. Moreover, it should be pointed out that loading process may cause plastic strains, which are also contemplated in the model. Some of these results may be described by previous version of the model (Savi et al., 2002; Baêta-Neves et al., 2004), but are reproduced here again. For all simulations, stress-driving loadings are adopted.

Material properties related to plasticity, presented in Table 2, must be considered together with adjusted parameters presented in Table 1. These values are representatives of a typical Ni–Ti alloy (Baêta-Neves et al., 2004). Notice that all simulations consider only tensile response and, therefore, parameters related to compressive are not addressed here.

At first, pseudo-elastic effect is concerned regarding a SMA specimen subjected to an isothermal mechanical loading performed at $T = 373$ K ($T > T_A$). Fig. 4 presents the mechanical load and also the stress–strain curve. When the specimen is free of stress, the austenitic phase is stable. After this, positive stresses induce the formation of the $M+$ variant of martensite. The loading process continues until the yield surface is reached, developing plastic strains. The unloading process induces austenite formation again and, at the end of the loading–unloading process, the specimen presents an irreversible residual strain that cannot be eliminated by the reverse transformation.

Table 2
Model parameters related to plasticity for a Ni–Ti alloy (Baêta-Neves et al., 2004)

| $\sigma_Y^{A,i}$ (GPa) | $\sigma_Y^{A,f}$ (GPa) | $\sigma_Y^{M}$ (GPa) | $\eta_{ci}$ | $\eta_{ck}$ | $K_A$ (GPa) | $K_M$ (GPa) | $H_A$ (GPa) | $H_M$ (GPa) | $T_F$ (K) |
|---|---|---|---|---|---|---|---|---|---|
| 1.5 | 1.0 | 0.5 | −0.01 | −0.01 | 1.4 | 0.4 | 4 | 1.1 | 423 |

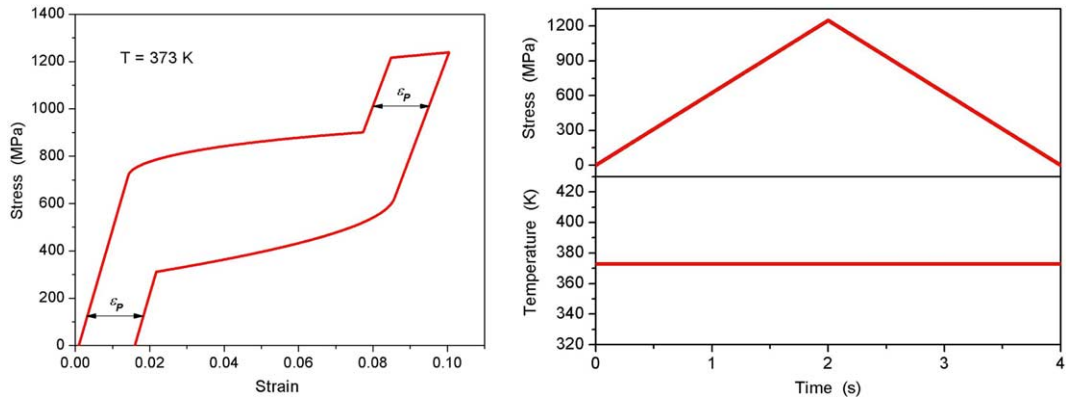


Fig. 4. Pseudoelasticity.

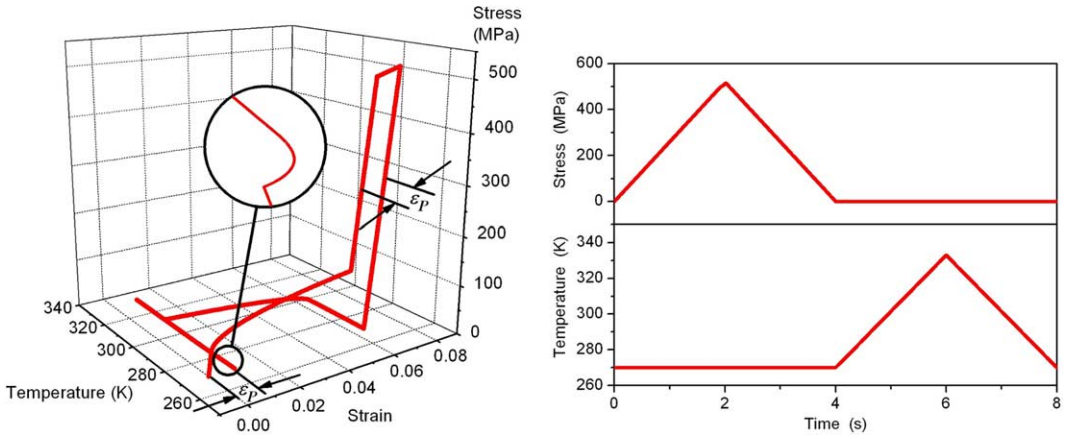


Fig. 5. One-way shape memory effect.

Shape memory effect is now focused regarding a thermomechanical load depicted in Fig. 5. Firstly, a constant temperature $T = 270$ K ($T < T_M$) is considered, where twinned martensite is a stable phase. After a mechanical loading is applied, the specimen experiences the phase transformation from twinned martensite, $M$ to detwinned martensite, $M+$. In this stage, loading process continues to be applied and the yield surface is reached. After that, unloading process promotes the elastic unloading which reveals the presence of residual strain. A subsequent heating process induces the transformation from detwinned martensite, $M+$, to the austenitic phase, $A$. Notice, however, that the plastic strain portion, induced by the plastification process, cannot be eliminated by the reverse phase transformation promoted by the thermal load. The detail in Fig. 5 reveals a region free of stress where phase transformation due temperature variation promotes a perturbation in the strain–temperature evolution. This behavior is associated with a temperature–strain hysteresis loop and is explored in more detail in the next example which involves a situation free of stress.

The phase transformation due to temperature variation is now considered regarding a thermal loading, free of stress. Fig. 6 presents the strain–temperature curve, showing thermal expansion and phase transformations related to a thermal loading. Notice the hysteretic characteristics of phase transformation.

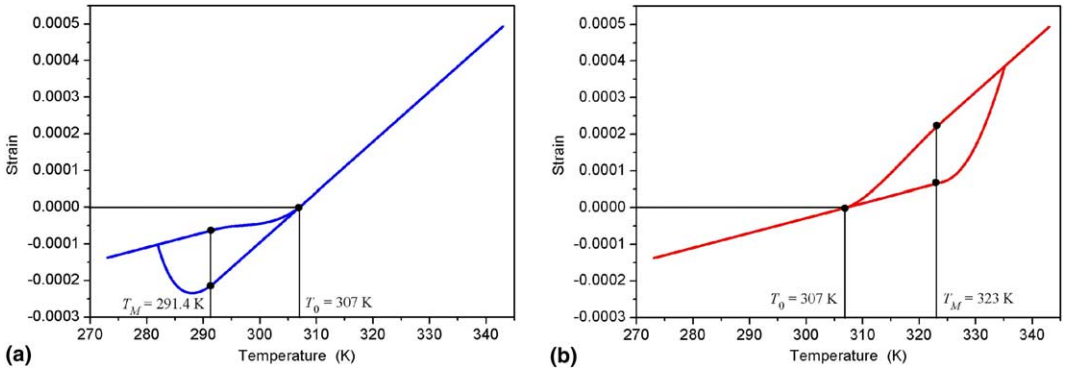


Fig. 6. Phase transformation due to temperature variation: (a) $T_M = 291.4$ K (positive two-way strain); (b) $T_M = 307.5$ K (negative two-way strain).

Experimental data presented by Jackson et al. (1972) show a similar curve, indicating that the model is capable to describe the coupling between shape memory effects and thermal expansion. Miller and Lagoudas (2000) use the term two-way strain to describe the strain developed during the austenitic to martensitic phase transformation under zero load. This strain is the result of dislocation arrangements and, typically, SMAs present positive two-way strains. In the cited reference, the authors show experimental tests that present negative values for these strains. Miller and Lagoudas present an argument that this apparent discrepancy with theory may be explained by a previous heat treatment of the specimen. Fig. 6 presents the difference between two curves obtained for different temperatures values of $T_M$. Since this temperature may be altered by heat treatments (Tang and Sandström, 1995), it is possible to see how this alteration modifies the phase transformation curves, changing the sign of two-way strain. Fig. 6a considers $T_M = 291.4$ K while Fig. 6b uses $T_M = 307.5$ K. Each curve has a different sign for two-way strain, showing that is possible to alter this sign by altering the phase transformation temperature.

Two-way shape memory effect is now considered (Bo and Lagoudas, 1999; Zhang et al., 1991). With this aim, stress-induced martensite training (SIM training), represented in Fig. 7, is simulated. Initially, twenty cycles of an isothermal mechanical process ($T = 373$ K), with increasing maximum values, is considered, causing plastic strains. After this mechanical process, thermal load is applied maintaining a constant value

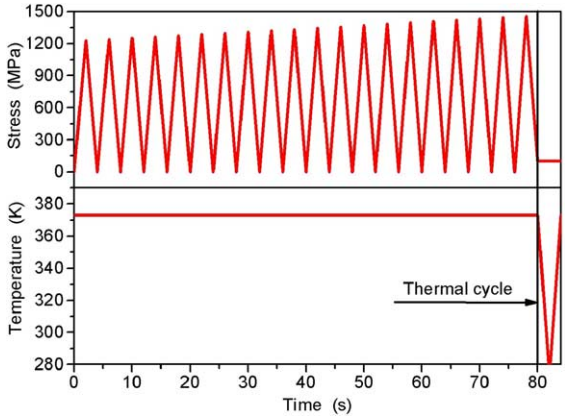


Fig. 7. Stress-induced martensite training (SIM training).

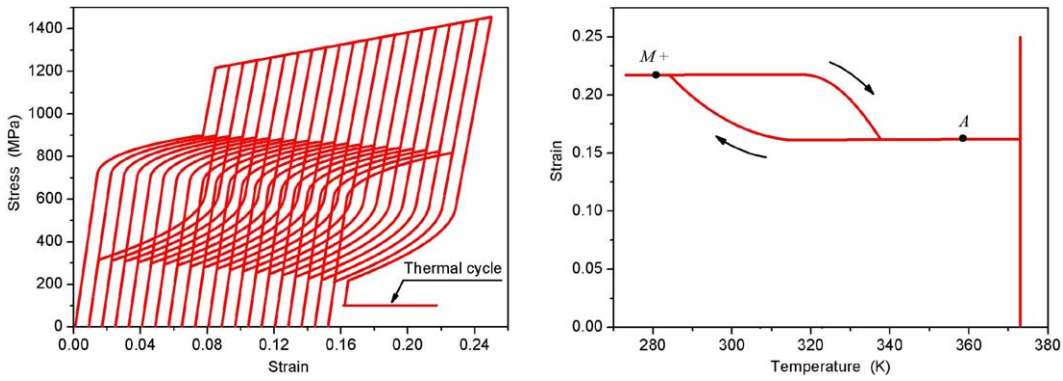


Fig. 8. Two-way shape memory effect.

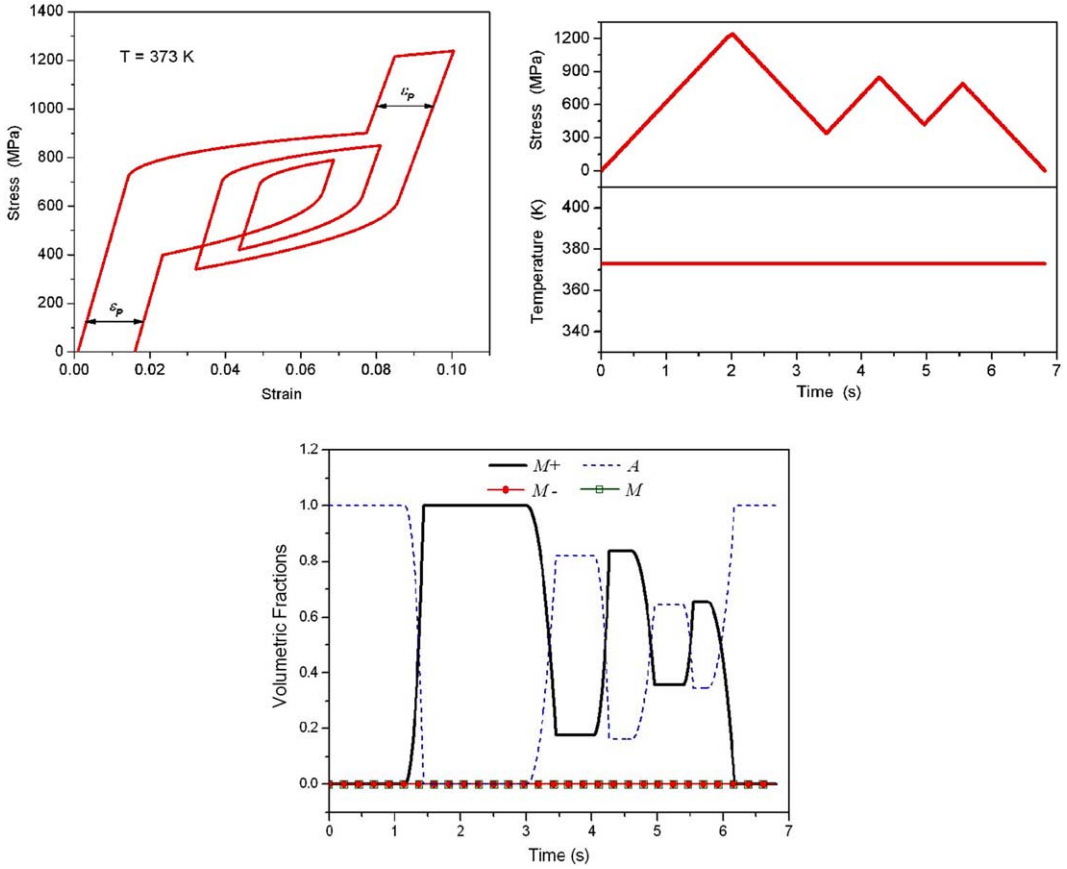


Fig. 9. Internal sub-loops due to incomplete phase transformations.

of mechanical load ($\sigma = 100$ MPa). Fig. 8 shows the stress–strain curve during SIM training. Notice the growth of plastic strains during each load cycle. Finished this process, SMA presents phase transformation $A \rightarrow M+$ during cooling and $M+ \rightarrow A$ during heating. This behavior is related to the two-way shape memory effect that allows one to associate each phase to a different form. Fig. 8 also shows a strain–temperature curve, representing this effect. It should be pointed out that the description of this phenomenon is related to the plastic-phase transformation coupling introduced in the proposed model (Savi et al., 2002).

Finally, internal sub-loops due to incomplete phase transformations is focused on considering a pseudoelastic problem, similar to the one presented in Fig. 4. Imposing a loading process shown in Fig. 9, it induces incomplete phase transformations. This is an important characteristics related to SMA response, which is captured by the proposed model. Fig. 9 also shown the volumetric fractions of the phases.

## 4. Tensile–compressive asymmetry

At this point, tensile–compressive asymmetry is focused on. With this aim, a SMA specimen is subjected to different thermomechanical loadings. Basically, stress-driving simulations are carried out considering tensile and compressive behaviors at a constant temperature. Moreover, it is assumed that all

simulations are performed without reaching the yield surface and, therefore, plastic parameters are not considered here.

Experimental results presented by Gall et al. (1999) are used as reference to calibrate numerical results obtained from the proposed model. In the experimental tests developed in the cited reference, single and polycrystal specimens with different orientation and subjected to different aging treatments are analyzed. The aging treatment causes $Ti_3Ni_4$ precipitation, being related to the tension–compression asymmetry. Basically, these precipitates act as nucleation sites for martensite and obstacles for dislocation motion. This mechanism effectively increases the critical stress for dislocation motions and decreases the critical stress for phase transformation.

Here, numerical simulations related to some of these tests are carried out, showing the potentiality of the proposed model. Figures are plotted considering absolute values of stress and strain for compressive tests. At first, a single crystal aged 1.5 h at 673 K (peak-aged) is considered. The parameters presented in Table 3 are used for the numerical simulations. Under this condition, compressive behavior presents small values of critical stress, where phase transformation begins to take place, and also smaller residual strain. The model response captures this behavior as shown in Fig. 10a. On the other hand, tensile behavior is quite different. Numerical and experimental results are in agreement except for the response during unloading in tensile behavior. Gall et al. (1999) say that this behavior indicates that transformation product is unstable under tensile unloading.

Fig. 10b shows the same test related to a different aging treatment, namely aged 15 h at 773 K (over-aged), which the specimen is subjected before the test. Table 4 presents the employed parameters. Notice that different set of parameters are considered in order to describe the response of the SMA after aging

Table 3
Thermomechanical properties: peak-aged single crystal [1 1 1] orientation, aged 1.5 h at 673 K

| $E_A$ (GPa) | $E_M$ (GPa) | $\alpha^T$ (MPa) | $\alpha^C$ (MPa) | $\varepsilon_R^T$ | $\varepsilon_R^C$ | $L_0^T$ (MPa) | $L^T$ (MPa) | $L_0^C$ (MPa) | $L^C$ (MPa) | $L_0^A$ (MPa) | $L^A$ (MPa) |
|---|---|---|---|---|---|---|---|---|---|---|---|
| 36.5 | 107 | 4044 | 1520 | 0.0663 | −0.0227 | 18.95 | 273.06 | 12.85 | 402.96 | 11.95 | 456 |
| $\Omega_A$ (MPa/K) | $\Omega_M$ (MPa/K) | $T_M$ (K) | $T_A$ (K) | $T_0$ (K) | $\eta_1^L$ (MPa s) | $\eta_1^U$ (MPa s) | $\eta_2^L$ (MPa s) | $\eta_2^U$ (MPa s) | $\eta_3^L$ (MPa s) | $\eta_3^U$ (MPa s) | |
| 0.74 | 0.17 | 273.5 | 317.5 | 295 | 6.02 | 6.02 | 4.09 | 4.09 | 3.8 | 3.8 | |

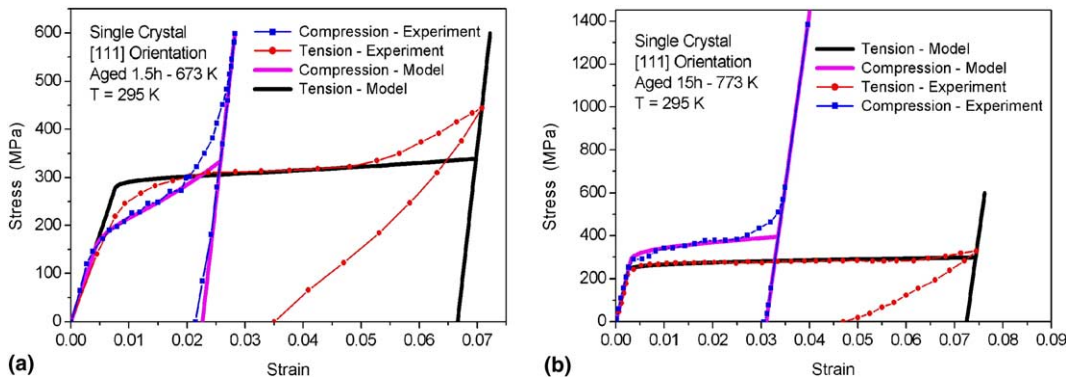


Fig. 10. Stress–strain curves for a single crystal with [1 1 1] orientation: (a) aged 1.5 h at 673 K; (b) aged 15 h at 773 K.

Table 4
Thermomechanical properties: over-aged single crystal [1 1 1] orientation, aged 15 h at 773 K

| $E_A$ (GPa) | $E_M$ (GPa) | $\alpha^T$ (MPa) | $\alpha^C$ (MPa) | $\varepsilon_R^T$ | $\varepsilon_R^C$ | $L_0^T$ (MPa) | $L^T$ (MPa) | $L_0^C$ (MPa) | $L^C$ (MPa) | $L_0^A$ (MPa) | $L^A$ (MPa) |
|---|---|---|---|---|---|---|---|---|---|---|---|
| 94 | 161 | 2250 | 1670 | 0.0723 | −0.0311 | 12.51 | 209.55 | 9.5 | 300.25 | 13.34 | 456 |
| $\Omega_A$ (MPa/K) | $\Omega_M$ (MPa/K) | $T_M$ (K) | $T_A$ (K) | $T_0$ (K) | $\eta_1^L$ (MPa s) | $\eta_1^U$ (MPa s) | $\eta_2^L$ (MPa s) | $\eta_2^U$ (MPa s) | $\eta_3^L$ (MPa s) | $\eta_3^U$ (MPa s) | |
| 0.74 | 0.17 | 271.2 | 301.7 | 295 | 1.91 | 1.91 | 2.063 | 2.063 | 2 | 2 | |

treatment. Again, experimental and numerical results are in agreements. The aging treatment alters the response of the specimen changing the slope of the phase transformation region. Gall et al. (1999) say that either tension–compression asymmetry or orientation dependence of the stress–strain response are strongly related to heat treatments (precipitate sizes).

The forthcoming analysis considers a polycrystal SMA with $\langle 1\,1\,1\rangle\{1\,1\,0\}$ texture (Fig. 11). Results are qualitatively similar to the previous one related to single crystals. Since the proposed model is related to phenomenological features, the results demonstrate the model ability in describing both single and polycrystals behavior. It should be pointed out, however, that a different set of parameters is being considered for the description of polycrystals. The use of the same set of parameters needs a proper formulation (Thamburaja and Anand, 2001). Table 5 presents parameters used for the peak-aged polycrystal specimen

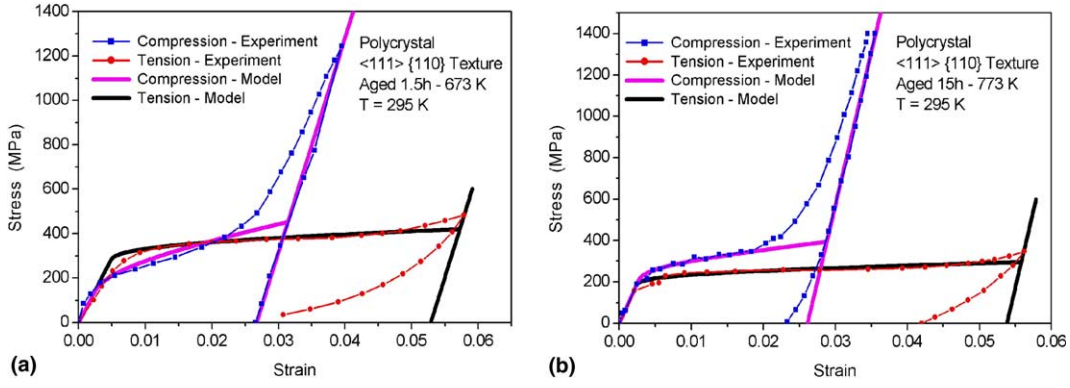


Fig. 11. Stress–strain curves for a polycrystal with $\langle 1\,1\,1\rangle\{1\,1\,0\}$ texture: (a) aged 1.5 h at 673 K; (b) aged 15 h at 773 K.

Table 5
Thermomechanical properties: peak-aged polycrystal $\langle 1\,1\,1\rangle\{1\,1\,0\}$ texture, aged 1.5 h at 673 K

| $E_A$ (GPa) | $E_M$ (GPa) | $\alpha^T$ (MPa) | $\alpha^C$ (MPa) | $\varepsilon_R^T$ | $\varepsilon_R^C$ | $L_0^T$ (MPa) | $L^T$ (MPa) | $L_0^C$ (MPa) | $L^C$ (MPa) | $L_0^A$ (MPa) | $L^A$ (MPa) |
|---|---|---|---|---|---|---|---|---|---|---|---|
| 58 | 96.5 | 1817 | 910 | 0.0527 | −0.0268 | 12.16 | 148.2 | 14.42 | 311.27 | 15 | 360 |
| $\Omega_A$ (MPa/K) | $\Omega_M$ (MPa/K) | $T_M$ (K) | $T_A$ (K) | $T_0$ (K) | $\eta_1^L$ (MPa s) | $\eta_1^U$ (MPa s) | $\eta_2^L$ (MPa s) | $\eta_2^U$ (MPa s) | $\eta_3^L$ (MPa s) | $\eta_3^U$ (MPa s) | |
| 0.74 | 0.17 | 262.2 | 314 | 295 | 5.7 | 5.7 | 6.75 | 6.75 | 7 | 7 | |

Table 6
Thermomechanical properties: over-aged polycrystal $\langle 1\,1\,1\rangle\{1\,1\,0\}$ texture, aged 15h at 773 K

| $E_A$ (GPa) | $E_M$ (GPa) | $\alpha^T$ (MPa) | $\alpha^C$ (MPa) | $\varepsilon_R^T$ | $\varepsilon_R^C$ | $L_0^T$ (MPa) | $L^T$ (MPa) | $L_0^C$ (MPa) | $L^C$ (MPa) | $L_0^A$ (MPa) | $L^A$ (MPa) |
|---|---|---|---|---|---|---|---|---|---|---|---|
| 78 | 148 | 1880 | 1443 | 0.0538 | −0.0262 | 12.1 | 196.27 | 13.4 | 300.06 | 12.39 | 360 |
| $\Omega_A$ (MPa/K) | $\Omega_M$ (MPa/K) | $T_M$ (K) | $T_A$ (K) | $T_0$ (K) | $\eta_1^L$ (MPa s) | $\eta_1^U$ (MPa s) | $\eta_2^L$ (MPa s) | $\eta_2^U$ (MPa s) | $\eta_3^L$ (MPa s) | $\eta_3^U$ (MPa s) | |
| 0.74 | 0.17 | 273.8 | 305.8 | 295 | 3.24 | 3.24 | 3.58 | 3.58 | 3.3 | 3.3 | |

(aged 1.5 h at 673 K). Fig. 11a shows the numerical simulation together with experimental data. Notice that numerical and experimental results are in good agreement as well as in the single crystals simulations.

Finally, Fig. 11b shows results related to an over-aged polycrystal (aged 15 h at 773 K). Parameters are presented in Table 6. Again, results present qualitatively the same behavior compared to those related to single crystal response, showing quantitative agreements between numerical and experimental data.

## 5. Conclusions

The description of the thermomechanical behavior of shape memory alloys involves different and complex phenomena. Among others, plastic strain and thermo-plastic-phase transformation coupling are some of these behaviors. This article proposes a constitutive model that is capable to describe different aspects of SMA behavior. This constitutive model is based on previous contribution of Savi et al. (2002) and Baêta-Neves et al. (2004) that is built upon the contribution of Fremond (1987, 1996). The model includes four macroscopic phases in the formulation and different material parameters for each phase, which allows one to represent tensile–compressive asymmetry. Thermal expansion and plastic strains are also included into the formulation. Hardening effect is represented by a combination of kinematic and isotropic behaviors and a plastic-phase transformation coupling is considered. The horizontal enlargement of the stress–strain hysteresis loop is considered in order to allow better adjustments with experimental data. Comparisons between numerical and experimental results show that they are in close agreement. Numerical results also show that the proposed model is capable to capture the general behavior of experimental data, presenting a proper description of different phenomena as pseudo-elasticity, one-way and two-way shape memory effects, phase transformation due to temperature variation, internal sub-loops due to incomplete phase transformations and tensile–compressive asymmetry effects.

## Acknowledgments

The authors acknowledge the support of the Brazilian Agencies CNPq and CAPES.

## References

Baêta-Neves, A.P., Savi, M.A., Pacheco, P.M.C.L., 2004. On the Fremond's constitutive model for shape memory alloys. Mechanics Research Communications 31 (6), 677–688.

Birman, V., 1997. Review of mechanics of shape memory alloy structures. Applied Mechanics Review 50, 629–645.

Bo, Z.H., Lagoudas, D.C., 1999. Thermomechanical modeling of polycrystalline SMAs under cyclic loading, Part III: evolution of plastic strains and two-way shape memory effect. International Journal of Engineering Science 37, 1175–1203.

Denoyer, K.K., Erwin, R.S., Ninneman, R.R., 2000. Advanced smart structures flight experiments for precision spacecraft. Acta Astronautica 47, 389–397.

Duerig, T., Pelton, A., Stöckel, D., 1999. An overview of nitinol medical applications. Materials Science and Engineering A 273–275, 149–160.

Fremond, M., 1987. Matériaux à Mémoire de Forme, C.R. Acadamic Science, Paris, Tome 34, s.II, n.7, pp. 239–244.

Fremond, M., 1996. Shape Memory Alloy: A Thermomechanical Macroscopic Theory, CISM courses and lectures. Springer Verlag.

Gall, K., Sehitoglu, H., Chumlyakov, Y.I., Kireeva, I.V., 1999. Tension–compression asymmetry of the stress–strain response in aged single crystal and polycrystalline NiTi. Acta Materialia 47 (4), 1203–1217.

Gall, K., Sehitoglu, H., 1999. The role of texture in tension–compression asymmetry in polycrystalline NiTi. International Journal of Plasticity 15, 69–92.

Garner, L.J., Wilson, L.N., Lagoudas, D.C., Rediniotis, O.K., 2001. Development of a shape memory alloy actuated biomimetic vehicle. Smart Materials and Structures 9 (5), 673–683.

Jackson, C.M., Wagner, H.J., Wasilewski, R.J., 1972. 55-Nitinol—The Alloy with a Memory: Its Physical Metallurgy, Properties, and Applications. NASA-SP-5110.

James, R.D., 2000. New materials from theory: trends in the development of active materials. International Journal of Solids and Structures 37, 239–250.

Lagoudas, D.C., Entchev, P.B., Kumar, P.K., 2003. Thermomechanical characterization SMA actuators under cyclic loading. Proceedings of IMECE'03, 2003 ASME International Mechanical Engineering Congress, Washington, DC, November 15–21.

Lagoudas, D.C., Rediniotis, O.K., Khan, M.M., 1999. Applications of shape memory alloys to bioengineering and biomedical technology, Proceedings of 4th International Workshop on Mathematical Methods in Scattering Theory and Biomedical Technology, October 1999, Perdika, Greece.

Lemaitre, J., Chaboche, J.-L., 1990. Mechanics of Solid Materials. Cambridge University Press.

Machado, L.G., Savi, M.A., 2002. Odontological applications of shape memory alloys. Revista Brasileira de Odontologia 59 (5), 302–306, in portuguese.

Machado, L.G., Savi, M.A., 2003. Medical applications of shape memory alloys. Brazilian Journal of Medical and Biological Research 36 (6), 683–691.

Miller, D.A., Lagoudas, D.C., 2000. Thermo-mechanical Characterization of NiTiCu and NiTi SMA actuators: influence of plastic strains, smart. Materials and Structures 5, 640–652.

Ortiz, M., Pinsky, P.M., Taylor, R.L., 1983. Operator split methods for the numerical solution of the elastoplastic dynamic problem. Computer Methods of Applied Mechanics and Engineering 39, 137–157.

Otsuka, K., Ren, X., 1999. Recent developments in the research of shape memory alloys. Intermetallics 7, 511–528.

Pacheco, P.M.C.L., Savi, M.A., 1997. A non-explosive release device for aerospace applications using shape memory alloys, Proceedings of XIV the Brazilian Congress of Mechanical Engineering (COBEM 97—ABCM), Bauru, Brazil.

Paiva, A., 2004. Modeling of Thermomechanical Behavior of Shape Memory Alloys, Ph.D. Thesis, PUC-Rio, Department of Mechanical Engineering (in portuguese).

Rockafellar, R.T., 1970. Convex Analysis. Princeton Press.

Rogers, C.A., 1995. Intelligent Materials. Scientific American (September), 122–127.

Savi, M.A., Braga, A.M.B., 1993. Chaotic vibrations of an oscillator with shape memory. Journal of the Brazilian Society for Mechanical Sciences XV (1), 1–20.

Savi, M.A., Paiva, A., Baêta-Neves, A.P., Pacheco, P.M.C.L., 2002. Phenomenological modeling and numerical simulation of shape memory alloys: a thermo-plastic-phase transformation coupled model. Journal of Intelligent Material Systems and Structures 3 (5), 261–273.

Schroeder, T.A., Wayman, C.M., 1977. The formation of martensite and the mechanism of the shape memory effect in single crystals of Cu–Zn alloys. Acta Metallurgica 25, 1375.

Shaw, J.A., Kyriakides, S., 1995. Thermomechanical Aspects of NiTi. Journal of Mechanics Physics Solids 43, 1243–1281.

Simo, J.C., Hughes, T.J.R., 1998. Computational Inelasticity. Springer.

Tang, W., Sandström, R., 1995. Limitations of constitutive relations for TiNi shape memory alloys. Journal de Physique IV 5, 185–190, C8.

Thamburaja, P., Anand, L., 2001. Polycrystalline shape-memory materials: effect of crystallographic texture. Journal of the Mechanics and Physics of Solids 49, 709–737.

Tobushi, H., Iwanaga, N., Tanaka, K., Hori, T., Sawada, T., 1991. Deformation behavior of Ni–Ti shape memory alloy subjected to variable stress and temperature. Continuum Mechanics and Thermodynamics 3, 79–93.

van Humbeeck, J., 1999. Non-medical applications of shape memory alloys. Materials Science and Engineering A 273–275, 134–148.

Webb, G., Wilson, L., Lagoudas, D.C., Rediniotis, O., 2000. Adaptive control of shape memory alloy actuators for underwater biomimetic applications. AIAA Journal 38 (2), 325–334.

Zhang, X.D., Rogers, C.A., Liang, C., 1991. Modeling of two-way shape memory effect. ASME—Smart Structures and Materials 24, 79–90.